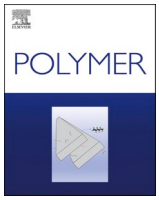
Polymer 342 (2026) 129319



Contents lists available at ScienceDirect

Polymer

journal homepage: www.elsevier.com/locate/polymer





Cure kinetics, glass transition and chemoviscosity models for an aerospace-grade disulphide-based benzoxazine vitrimer

Festus Ifeanyi Anagwu *, Daniel Preston, Alex A. Skordos

Composites and Advanced Materials Centre, School of Aerospace, Transport and Manufacturing, Cranfield University, Cranfield, MK43 0AL, United Kingdom

ARTICLE INFO

Keywords:
Composites
Polybenzoxazine vitrimer
Cure kinetics
Modelling
Chemorheology

ABSTRACT

This study reports the matrix material models for the manufacturing of reinforced fibre composites using a disulphide-enabled aerospace-grade benzoxazine vitrimer. Cure kinetics and chemoviscosity models, crucial for fibrous composite manufacturing optimisation, were developed using calorimetric and rheometric data, respectively. An autocatalytic model with a logistic term accounting for diffusion represents accurately the resin cure kinetics, with 4 % average relative error in degree of cure prediction. The glass transition (T_g) evolution follows the DiBenedetto equation, with a curvature parameter (λ) of 1.84. A chemorheological model based on the kinetics of viscosity at a reference temperature and an inverse temperature exponential dependence—appropriate for low degrees of cure prevailing during the filling/consolidation step of fibrous composite manufacturing—simulates rheological behaviour with an average error of 8.3 %. The initial viscosity ranges from 144.7 mPa·s at 130°C to 1119 mPa·s at 100°C, with fast evolution which limits impregnation, meaning that composites processing using a resin film infusion or pre-impregnation route is applicable to this vitrimeric matrix.

1. Introduction

Benzoxazines have been proposed as viable options for achieving low-pressure reprocessing of high temperature vitrimer composites [1], which is a challenge for high temperature epoxy vitrimer composites [2]. To manufacture high quality vitrimer composites, the processing must be optimised to permit precise control of product quality whilst ensuring minimisation of manufacturing cost. An optimal manufacturing system ensures shorter cycle times and prevents both incomplete crosslinking due to inadequate cure and material degradation due to excessive heating. It helps to achieve products devoid of dry spots or voids, reduced energy consumption, low residual stress, and higher production rates relative to suboptimal manufacturing conditions.

Process optimisation requires an understanding of the real-time state of crosslinking during cure [3,4]. Similarly to conventional thermoset matrices, the cure of vitrimers may be accompanied by phenomena such as thermal gradients and temperature overshoots [5–7]. These issues arise from heat generation in the interior of thick laminates, a consequence of the exothermic reaction and of the low thermal conductivity of the composite in the through thickness direction [8]. The result is inhomogeneity of cure and high residual stresses in the manufactured component. Matrix cure shrinkage, thermal expansion and contraction mismatch between layers result in residual stress development in the composite which affects final product quality by introducing microcracks and process distortion [9–13]. These are controlled by the manufacturing conditions and serve as potential initiation points for in-service failure of structural components. Furthermore, excessive heating leads to material degradation, lowering the glass transition temperature and potentially affecting mechanical performance, whilst incomplete or non-uniform curing compromises the desired quality and reliability of the manufactured part as well as its environmental resistance [14].

It is necessary to prioritise cure optimisation to prevent defects in manufactured parts. This ensures the final product meets the intended performance and reliability [15–17], thereby guaranteeing operational safety. The design of the process is governed by the kinetics of crosslinking, capturing the oxazine ring-opening polymerisation step, the kinetics of crosslinking of any accompanying functional group present, and any effects of the bond exchange mechanism that might occur if the cure temperature reaches the topology freezing temperature (T_v) of the vitrimer [3]. For any temperature profile, the cure kinetics model,

* Corresponding author.
E-mail addresses: f.i.anagwu@cranfield.ac.uk (F.I. Anagwu), Daniel.Preston.633@cranfield.ac.uk (D. Preston), a.a.skordos@cranfield.ac.uk (A.A. Skordos).

https://doi.org/10.1016/j.polymer.2025.129319
Received 31 July 2025; Received in revised form 27 October 2025; Accepted 8 November 2025
Available online 9 November 2025
0032-3861/© 2025 The Authors. Published by Elsevier Ltd. This is an open access article under the CC BY license (http://creativecommons.org/licenses/by/4.0/).

coupled with the knowledge of glass transition temperature (T_g) dependence on degree of cure, allows an accurate tracking of material state.

Optimising vitrimer composite manufacturing requires an understanding of both the temperature-dependent matrix flow during consolidation and the heat transfer dynamics during curing. To achieve this, accurate cure kinetics and chemorheological models must be developed to simulate effectively the infusion, consolidation, and curing stages. The exothermic heat of the curing reaction—which has net zero contribution from the vitrimer dynamic bond exchange reaction—is used to simulate the energy balance in heat transfer modelling, whilst constitutive models for degree of cure-dependent properties such as thermal conductivity, heat capacity, curing material modulus and coefficient of thermal expansion require an underlying cure kinetics model.

Polybenzoxazines are not as widely used as epoxies in fibre-reinforced composites, primarily due to their inferior toughness, an improvement of which has been the subject of considerable research efforts with potentially positive results [18,19]. Cure and chemorheological models for optimal manufacturing of benzoxazine-based composites are few in literature, all of which confirm autocatalysis [20–26]. However, there is no process model or dataset available for optimal manufacturing of benzoxazine-based fibrous vitrimer composites. This work develops the cure kinetics, glass transition temperature evolution, and rheological behaviour models for an established aerospace-grade benzoxazine vitrimer incorporating disulphide bond, reported in Ref. [27]. The documented characteristics of this vitrimer—such as glass transition temperature higher than 140°C normally required for aerospace-grade resins and environmental performance comparable to aerospace epoxies—are indicative of the applicability of this resin to aeronautics. Cure and glass transition advancement data were collected using differential scanning calorimetry (DSC). Chemoviscosity data were generated by isothermal flow rheometry. Fitting of the proposed models to the experimental data was utilised to determine their parameters, delivering constitutive models adequate for the process optimisation of composites of the vitrimer matrix system.

2. Materials and methods

2.1. Materials

Bis(4-hydroxyphenyl) disulphide (CAS number: 15015573; 98 %), aniline (CAS number: 62533; 99.8 %), and paraformaldehyde (CAS number: 30525894) were supplied by AmBeed USA, Fisher Scientific, and Sigma Aldrich/Merck, respectively. All chemicals were used as received from the suppliers. The recently proposed aerospace-grade disulphide-based benzoxazine vitrimer (DHPDS-a) [27] was solventlessly synthesised following the procedure reported in Ref. [27]. The benzoxazine vitrimer monomer was synthesised from analytical-grade precursors using the one-pot solventless method, which yields high-purity monomers requiring no further purification provided stoichiometric precursor ratios are employed, and the precursors are introduced in the right order in the reaction vessel. Characterisation of the monomer has been published previously [27]. FTIR spectra show no signals attributable to impurities, whilst NMR reveals only minor oligomeric benzoxazine species arising from oxazine ring pre-opening during synthesis. These oligomers do not severely influence the curing mechanism, but they may account for a non-zero initial degree of cure. In addition to these, the repeatability of results is confirmed from the results of repeat experiments presented in Fig. S1–S3 in supplementary material. Briefly, 2.4 g paraformaldehyde was added to 3.72 g aniline and stirred at room temperature for 10 min. Bis(4-hydroxyphenyl) disulphide (5 g) was added at room temperature, and the mixture was heated to 90°C stirring at 300 rpm for 30 min to obtain a brown viscous benzoxazine monomer requiring no purification.

2.2. Experimental methods

DHPDS-a was cured in the TGA to assess the amount of weight loss of the material after full cure. The experiment was performed on a TGA 550 discovery (TA Instruments) under air atmosphere at 40 mL/min using a 100 μL platinum pan. The thermal programme consists of a dynamic ramp at 1°C/min from 25°C to 180°C, an isothermal dwell for 4 h at 180°C, a further dynamic ramp at 1°C/min from 180°C to 220°C, and a final isothermal dwell of 30 min at 220°C, to achieve full cure of the resin. The isothermal step at 220°C was followed by a jump to 35°C.

The cure behaviour of DHPDS-a was studied using a DSC 250 Discovery (TA Instruments) equipped with an RCS cooling system under nitrogen purge at 50 mL/min. An amount of resin in the range 5–10 mg was encapsulated in a Tzero aluminium pan and used to perform each DSC experiment. The 5–10 mg sample mass range ensures negligible thermal gradients. Heat flow values were normalised using the actual sample mass. Dynamic and isothermal DSC experiments with varying thermal profiles were performed. Dynamic DSC experiments were carried out at 2.5, 5 and 10°C/min heating rates and isothermal DSC experiments at 150, 160, 170, 180 and 190°C. For all isothermal DSC runs, the sample was brought to the desired temperature of the reaction using a10°C/min heating rate from -50°C, and the isothermal conditions were maintained until the DSC heat flow signal reached a plateau, signifying the end of the reaction. This was followed by quenching to -50°C and reheating up to 250°C at 10°C/min to identify any residual cure.

The initial reaction heat was considered in the integration of isothermal experiments, estimated using the results of the dynamic experiment at 10°C/min. The total heat of reaction (ΔH_T) was calculated by averaging the total heat of reaction for all experiments for which the residual reaction upon re-heating was negligible. A linear baseline was used to integrate DSC signals in dynamic experiments and a horizontal baseline in isothermal experiments to determine the heat of reaction and the evolution of reaction rate.

The glass transition temperature development during cure was investigated under 10 °C/min dynamic ramp using 10 partially cured samples comprising material cured dynamically at 1.25°C/min from −50°C to 146, 153, 158, 162, 167, 173, 179, 185 and 194°C, and material cured at 170°C for 120 min; material cured at 190°C for 30 min and an uncured sample.

Chemorheological data used in modelling the chemoviscosity evolution of DHPDS-a were obtained using an AR2000ex rheometer (TA Instruments), equipped with a water-cooling system. A cone and plate configuration involving a 40 mm diameter cone with a 2° angle and a truncation depth of 54 μm was used. The gap setting of the rheometer was adjusted to match the cone truncation depth. Chemoviscosity development in the resin was studied in four isothermal experiments at 100, 110, 120 and 130°C using a constant shear rate of 300 s^{-1}. The sample was loaded onto the lower plate of the rheometer, initially at ambient temperature, the gap was closed, and the temperature was equilibrated to the desired isothermal temperature for 30 s before shearing.

The rheological behaviour of DHPDS-a during advanced stages of the cure was investigated using a Discovery HR-20 Hybrid Rheometer (TA Instruments) equipped with a parallel plate geometry (disposable plates) and an Environmental Test Chamber (ETC) for precise temperature control. Measurement was performed under isothermal conditions at 130 and 150°C. The sample was degassed prior to the measurement. After loading and trimming, the sample was equilibrated at the set temperature before initiating oscillatory measurements. A constant strain of 0.1 % and a frequency of 0.5 Hz were applied throughout each experiment. The plate gap was maintained at 0.5 mm, and the minimum torque sensitivity was set to 5 μNm. The experiment was stopped when the viscosity exceeded 135,000 Pa·s.

2.3. Modelling methods

In DSC studies, where the same reactive groups per molecule are consistently transformed during curing, the heat released per cross-link remains constant. Under these conditions, the rate of chemical reaction is assumed proportional to the heat flow measured by the DSC. Consequently, the total heat released is proportional to the extent of reaction, allowing the degree of cure to be determined from the cumulative heat flow. The integrated cure kinetics DSC data were utilised to obtain the degree of cure (α) as follows:

$$\alpha(t) = \frac{H(t)}{\Delta H_T} \tag{1}$$

where $H(t)$ is the integral of the DSC heat flow signal at time, t. Reaction rate evolution is computed by differentiating numerically degree of cure with respect to time.

$$\frac{d\alpha}{dt} = \frac{1}{\Delta H_T}\frac{dH(t)}{dt} \tag{2}$$

The cure kinetics model proposed by Karkanas [28] including independent autocatalytic and nth order terms was utilised, in combination with a logistic function representing effects of diffusion [29], to model the kinetics as follows:

$$\frac{d\alpha}{dt} = \frac{A_1 e^{-E_1/RT}(1-\alpha)^{n_1} + A_2 e^{-E_2/RT}\alpha^m(1-\alpha)^{n_2}}{1 + e^{C[\alpha-(\alpha_{c0}+\alpha_{cT}T)]}} \tag{3}$$

where E_1 and E_2 are the activation energies, A_1 and A_2 are the pre-exponential factors and n_1 and n_2 are the nth orders of the two kinetics terms, m is the autocatalytic order of the autocatalytic term, α_{cT} and α_{co} are coefficients controlling the critical degree of cure for diffusion as a function of temperature, C is a coefficient controlling the breadth of the transition to diffusion control and R is the universal gas constant.

The curing reaction involves a chemically controlled step, which dominates the kinetics for the greatest part of the process and a diffusion step, which becomes rate-controlling as the material approaches and undergoes vitrification. For vitrimeric systems, if the topology freezing temperature is lower than the cure temperature, the mechanism of dynamic bond exchange can affect the cure by providing greater mobility of reacting species. This influence is greater at the stage of the reaction where diffusion plays an important role and is likely to result in the material reaching a greater final degree of cure and a glass transition temperature closer to the ultimate T_g of the system compared to an equivalent non-vitrimeric formulation under the same conditions.

The DiBenedetto equation was used to model the glass transition temperature development as a function of the degree of cure as follows:

$$T_g(\alpha) = T_{g0} + \frac{\lambda\alpha(T_{g\infty} - T_{g0})}{1-\alpha(1-\lambda)} \tag{4}$$

where T_{g0} is the glass transition temperature of the prepolymer, $T_{g\infty}$ is the ultimate glass transition temperature of the fully cured vitrimer and λ is a fitting parameter that determines the degree of convexity of the dependence of glass transition temperature on the fractional conversion.

The chemoviscosity of a curing resin is influenced by two competing factors: the gradual increase in molecular weight and network density during crosslinking, which reduce chain mobility and increase viscosity; and the effect of temperature, which enhances molecular mobility and leads to a decrease in viscosity. The net evolution of viscosity reflects the interplay between these opposing effects. For any resin, the resultant response is captured in a chemorheological model, enabling precise control of flow during fibre impregnation. The approach reported in Ref. [3], which is appropriate for modelling the evolution of viscosity in the infusion/consolidation stage of composites processing is used. In this, the rate of change in viscosity at a reference temperature (T_r) is represented as:

$$\frac{d\ln\eta_r}{dt} = Ae^{-\frac{E}{RT}}\left(ln\frac{\eta_r}{\gamma}\right)^l \tag{5}$$

where A is the pre-exponential factor, E and l are the activation energy and order of the log reference viscosity kinetics respectively, and γ is a fitting parameter constrained below the initial value of the reference viscosity (η_r^o). The viscosity is computed using the reference viscosity and the following temperature dependence:

$$\eta = \eta_r e^{D\left(\frac{1}{T}-\frac{1}{T_r}\right)} \tag{6}$$

where D is a coefficient that controls the temperature sensitivity.

The fitting of the models to the experimental data to identify the cure kinetics, glass transition temperature and viscosity evolution was carried out by minimising the absolute error across all experimental points using the Generalised Reduced Gradient Nonlinear Optimisation method implemented in Microsoft Excel Solver [30]. In the cure kinetics fitting, the error for each DSC experiment was normalised by the maximum rate measured in the experiment to ensure equal importance of each test to avoid data under fast reaction conditions dominating the parameter estimation. For both cure kinetics and rheology, the error in each was also normalised by the number of points to avoid dominance of slow tests which produce a greater number of data points. The dataset of this study can be accessed at Figshare research data repository at [31].

3. Results and discussion

3.1. TGA analysis

The TGA curve of DHPDS-a benzoxazine monomer is shown in Fig. 1. After the 4 h isothermal heating at 180 °C, 98.6 % of the material remains, with the 1.4 % mass loss attributed to volatilisation of residual water in the prepolymer. Back-calculation of the reaction enthalpy, normalised to the mass of dry resin, yields 239.5 J/g. By comparison, the average enthalpy measured by DSC (discussed in the next section) is 236.2 J/g, corresponding to a difference of only 3 J/g, or approximately 1 % error, which lies within the standard deviation of DSC measurements. This negligible difference has minimal impact on the cure kinetics model developed in this study and does not affect its validity.

3.2. Cure kinetics

The isothermal and dynamic reaction rate curves of DHPDS-a are illustrated in Fig. 2. All dynamic and isothermal DSC experiments, except the 150 and 160°C tests, result in full cure of the material. The total heat of the reaction of DHPDS-a system is 236.2 ± 18.0 J/g, corresponding only to the enthalpy of the ring-opening polymerisation of

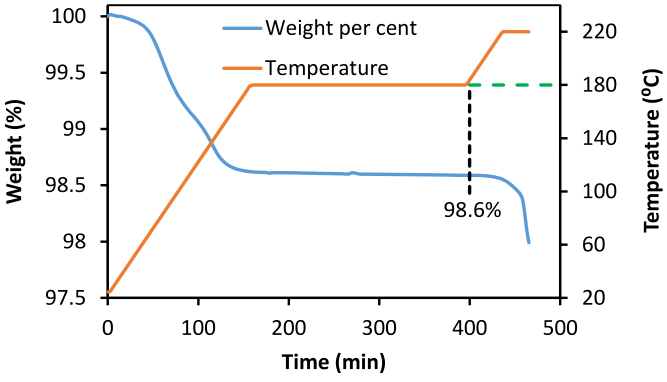


Fig. 1. TGA thermogram of DHPDS-a benzoxazine monomer.

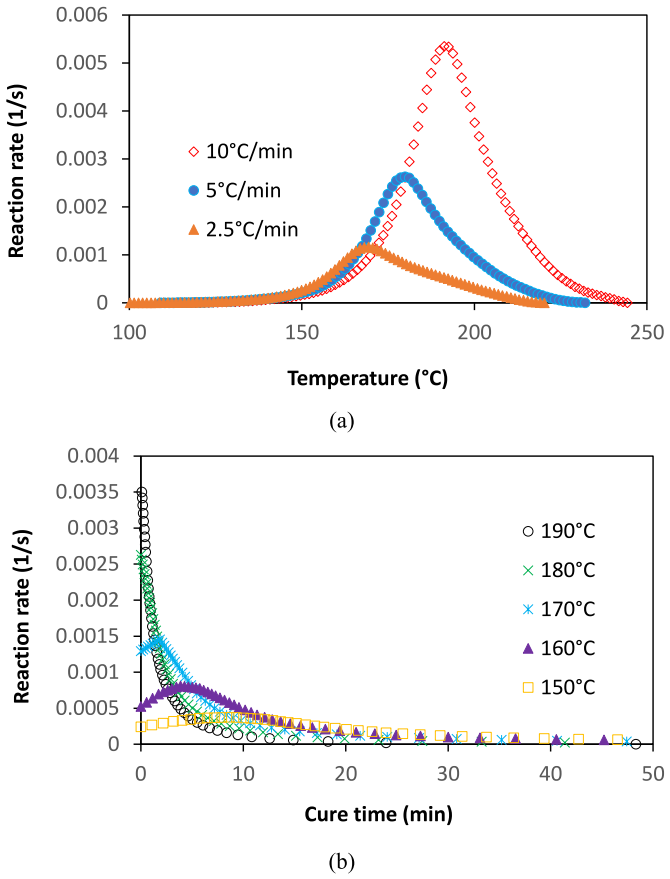


Fig. 2. Experimental cure kinetics of DHPDS-a system: (a) reaction rate versus temperature in dynamic DSC experiments; (b) reaction rate versus cure time in isothermal DSC experiments.

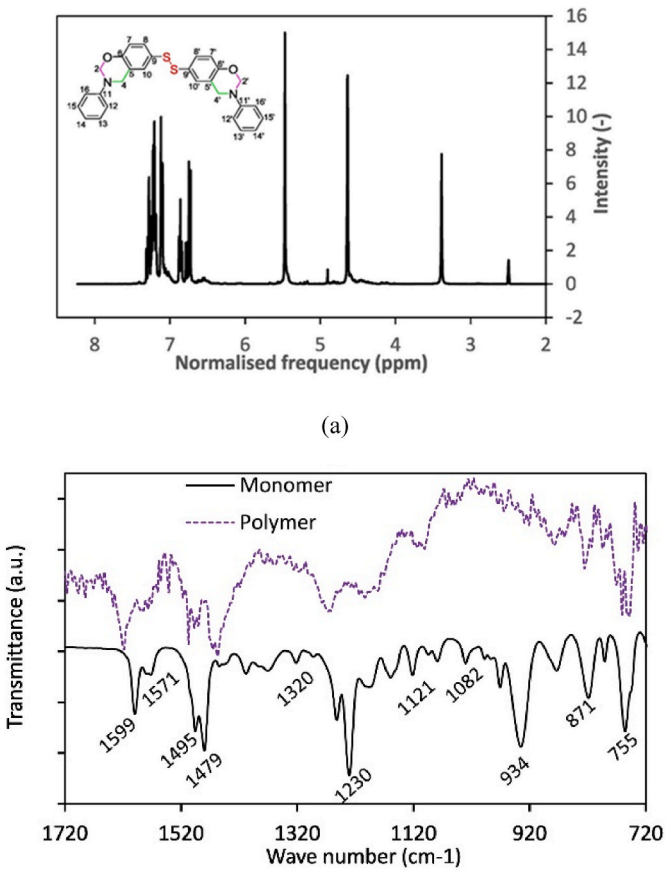


Fig. 3. ^{1}H NMR and FTIR spectra of DHPDS-a benzoxazine vitrimer. Reproduced from Ref. [27]. Copyright 2025, Elsevier.

the benzoxazine, as the net energy contribution from disulphide bond exchange during cross-linking is zero. Ishida reported the heat of reaction of a benzoxazine based on bisphenol-AF as 233.5 J/g [32].

Since each molecule of DHPDS-a contains two oxazine rings and has a molecular weight of 486.6 g/mol, the estimated heat of reaction per oxazine ring is 57 kJ/mol. Although, this compares with the range of 58.1–77.5 kJ/mol reported in Ref. [33], it is normally accepted that the heat of reaction of benzoxazine ring is 73 kJ/mol [20,34,35]. The value of 57 kJ/mol determined for DHPDS-a is likely slightly lower than the actual value, with the discrepancy attributed to the fact that part of the energy is lost in preopening some oxazine cycles during synthesis as mentioned in Ref. [27]. This can be seen in the ^{1}H NMR of DHPDS-a which is shown in Fig. 3(a), where two small broad peaks observed at 6.60 ppm and 7.20 ppm are attributed to the formation of oligomeric benzoxazines resulting from oxazine ring preopening during synthesis. No peak observed in the FTIR spectrum shown in Fig. 3(b) is assigned to any functional group absent in the molecular structure of DHPDS-a.

In dynamic data, a peak in reaction rate is observed at an intermediate conversion during the cure, attributed to the combined effects of temperature ramp and progression of the reaction. At the beginning of the reaction, the reaction rate increases in response to increasing temperature of the system, due to enhanced kinetic energy. The decline in the concentration of the reactants leads to a reduced frequency of molecular collisions. Therefore, the reaction rate increases with temperature until it reaches a maximum at an intermediate conversion point where the decline in reactant concentration dominates. Increasing the heating rate shifts the position of the reaction peak to the right, with the reaction peak temperature increasing from 169°C at 2.5°C/min to 191°C at 10°C/min, due to the shorter exposure to a specific temperature range with increasing heating rate. Similarly, the maximum rate increases with increasing rate from $1.2{\cdot}10^{-3}$ s^{-1} at 2.5°C/min to $5.3{\cdot}10^{-3}$ s^{-1} at 10°C/min, due to the occurrence of maxima at higher temperatures and the Arrhenius temperature dependence of the rate constant.

The autocatalytic character of DHPDS-a is confirmed from the peak of the reaction rate curves observed at intermediate conversions for isothermal experiments reported in Fig. 2(b). The duration of the isothermal reaction peaks decreases with increasing temperature, whilst the initial reaction rate has a finite value that increases with temperature. Maximum rates under isothermal conditions range from $3.8{\cdot}10^{-4}$ s^{-1} at 150°C to $3.5{\cdot}10^{-3}$ s^{-1} at 190°C, attributed to the Arrhenius temperature dependence of the rate constant. The calculation of the initial degree of cure for the isothermal experiments, reported in Table 1, was performed using the knowledge of the evolution of the cure from the corresponding dynamic test at 10°C/min. The isothermal cures at 180 and 190°C start from degree of cure of 29 % and 52 %, respectively; prior to attaining these degrees of cure, the reaction had proceeded past the peak rate during the dynamic ramp, thus eclipsing the manifestation of the autocatalytic character as a maximisation of reaction speed at intermediate times, as observed at lower temperatures.

An important observation in the cure kinetics of DHPDS-a benzox-

Table 1
Initial degree of cure of isothermal experiments reported in Fig. 2(b); isothermal temperature reached at a rate of 10°C/min.

Isothermal temperature (°C)	150	160	170	180	190
Degree of cure at time zero of the isothermal segment (–)	0.03	0.05	0.08	0.29	0.52
Final experimental degree of cure (–)	0.82	0.97	1.00	1.00	1.00

azine is the apparent role played by disulphide metathesis during the curing process. It was demonstrated that BA-a benzoxazine, which has similar structure with DHPDS-a except that the disulphide bond is replaced by a carbon atom bonded to two methyl groups, exhibits a T_g of 177.6°C, but is not fully cured at 190°C, 12.4°C above T_g [25]. At 180°C, which is above its T_g, it attains 0.81 fractional conversion. However, Table 1 reports that DHPDS-a with T_g of 155°C attains 0.82 fractional conversion below its T_g and nearly reaches full cure at 160°C, just 5°C above its T_g. Disulphide metathesis occurring even after vitrification provides the vitrified resin with some mobility allowing full cure to be attained closer to the ultimate T_g, which is not possible in a similar benzoxazine without the disulphide bond.

The superposition of dynamic and isothermal data, prepared by determining the degree of cure and reaction rate of dynamic data at the isothermal cure temperature, is illustrated in Fig. 4, confirming no path dependence of the system. The datapoints of Fig. 4 were determined by interpolating the reaction rate and degree of cure of the three dynamic heating rates of 2.5, 5, and 10°C/min at the isothermal temperatures of 150, 160, 170, 180 and 190°C, resulting in three datapoints that correspond to the three heating rates. The curves correspond to the reaction rate versus degree of cure of respective isothermal temperatures. The dynamic test results at the corresponding temperatures are in close agreement with the isothermal curves over the whole range. The average absolute difference between dynamic and isothermal rate data is $1.6{\cdot}10^{-4}$ s^{-1}, whilst the average relative difference is 12.7 %. Thus, a representation of the reaction rate as a unique function of degree of cure and temperature is applicable to DHPDS-a. This results also validates the assumption that the enthalpy measured by DSC provides a quantitative metric of the degree of conversion that is uniquely mapped to the state variables of the reaction.

Fig. 5 provides a comparison of experimental and model data for dynamic and isothermal experiments. Both dynamic and isothermal data are reproduced successfully by the cure kinetics model. The model overestimates the reaction rate at the beginning of high dynamic heating rates and underestimates it at higher temperatures to compensate for the initial overestimation. This is consistent with isothermal reaction rates in which the model estimates higher reaction rates at the beginning of the isothermal segments of high temperature experiments (180°C and 190°C) but adjusts closely to the experimental values as the reaction nears completion. This is also consistent with the superposition data presented in Fig. 4, in which isothermal reaction rates at the highest temperatures tend to be higher than the corresponding dynamic data points at the beginning. The model follows the rest of the experimental points closely, including the partial completion of cure, at about 0.82, in the lowest isothermal cure at 150°C and 0.97 at 160°C. The cure kinetics parameters identified by fitting the model to the experimental data are reported in Table 2.

Table 3 summarises the average absolute and relative error in reaction rate for each experiment. The absolute error ranges from $6.1{\cdot}10^{-6}$ s^{-1}

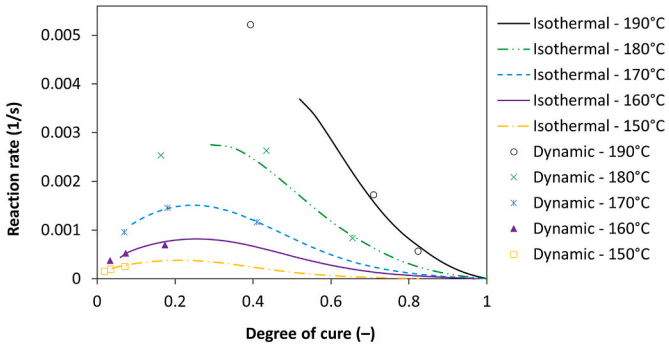


Fig. 4. Superposition of dynamic and isothermal reaction rate versus degree of cure data for DHPDS-a vitrimer.

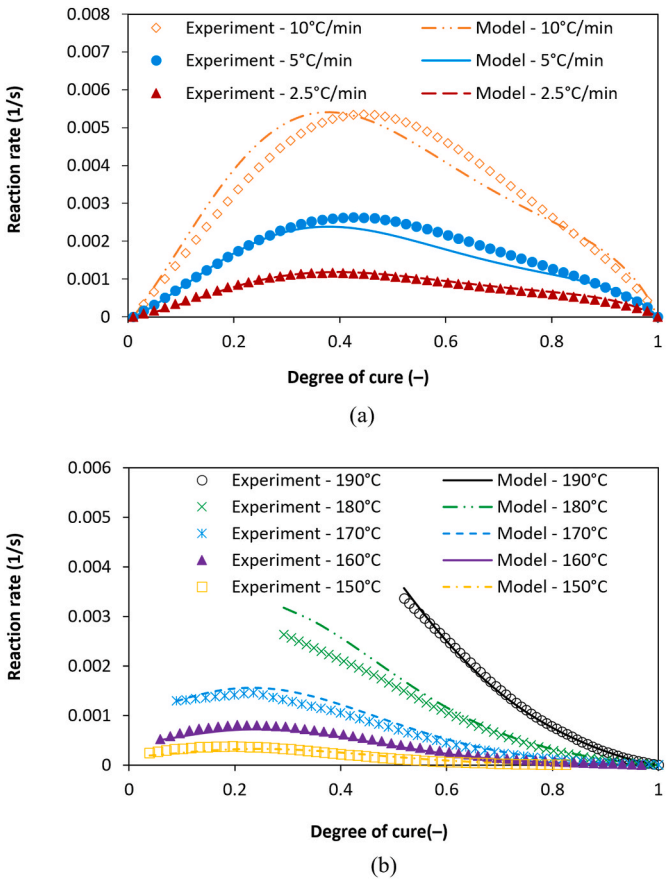


Fig. 5. Cure kinetics modelling of DHPDS-a: Comparison of model and experiment reaction rate in dynamic (a) and isothermal (b) conditions.

to $1.9{\cdot}10^{-4}$ s^{-1}, which in terms of relative error translates to 4.3 %–27.4 %. The average absolute error over all conditions is $4.2{\cdot}10^{-5}$ s^{-1}, and the relative error is 13.7 %. These errors are close to the superposition average absolute and relative differences of $1.6{\cdot}10^{-4}$ s^{-1} and 12.7 % respectively, indicating good performance of the model, as it represents the experimental results with an accuracy similar to the consistency of the dataset. Regression analysis of experimental reaction rates versus model reaction rates shows that the reaction rate error in the order of 12–14 % translates to a correlation coefficient (R^2) of 0.979. The absolute error in degree of cure ranges from 0.002 to 0.040 with corresponding relative error in the 0.2–10.7 % range. The reaction rate high relative errors of 20.6 % and 27.4 % for the 150 and 160°C isothermal DSC experiments do not compromise the overall model accuracy and reliability, given that the average relative error in degree of cure prediction reported in Table 3 is approximately 4.3 %. This is evident in Fig. 6 where the model overestimates slightly the experimental data in the diffusion-controlled regime of cure at 150°C but underestimates slightly at 160°C upon vitrification and diffusion limitation.

The validity of the cure kinetics model is tested by using it to predict the degree of cure evolution under isothermal and dynamic cure conditions, achieved by integrating the modelusing reaction rate data computed from Eq. (3) for the thermal profile of each experiment and comparing the model degree of cure with the corresponding experimental degree of cure. Fig. 6 illustrates these comparisons for dynamic and isothermal conditions. Fig. 6 includes 50 equally spaced degree of cure datapoints interpolated from experimental data to ensure no bias from data density. The model reproduces very closely the evolution of degree of cure in DSC experiments, with overall average absolute error in degree of cure across all experiments amounting to 0.015, corresponding to an overall relative error of 4.3 %. This model can form the

Table 2
DHPDS-a kinetics parameter values for the model represented by Eq. (3); α_o is the initial degree of cure used in the analysis.

α_o	A_1	E_1	n_1	A_2	E_2	n_2	m	C	α_{c0}	α_{cT}
(–)	(s^{-1})	J mol^{-1}	(–)	(s^{-1})	J mol^{-1}	(–)	(–)	(–)	(–)	(K^{-1})
0.01	$1.21{\cdot}10^{14}$	$1.45{\cdot}10^{5}$	1.32	$5.48{\cdot}10^{10}$	$1.03{\cdot}10^{5}$	4.63	1.81	6.21	−1.34	$1.44{\cdot}10^{-2}$

Table 3
Average absolute and relative errors in reaction rate and degree of cure of the cure kinetics model of DHPDS-a. Relative error computed over experimental points exceeding reaction rate of $2.5{\cdot}10^{-4}$ s^{-1}.

Experiment	Reaction rate		Degree of cure (–)	
	Absolute error	Relative error	Absolute error	Relative error
2.5 °C/min	$2.4{\cdot}10^{-5}$ s^{-1}	13.3 %	0.012	10.7 %
5 °C/min	$6.8{\cdot}10^{-5}s^{-1}$	11.2 %	0.009	5.7 %
10 °C/min	$1.9{\cdot}10^{-4}$ s^{-1}	18.0 %	0.010	5.7 %
150 °C	$1.1{\cdot}10^{-5}$ s^{-1}	20.6 %	0.030	4.8 %
160 °C	$1.8{\cdot}10^{-5}$ s^{-1}	27.4 %	0.040	4.8 %
170 °C	$6.1{\cdot}10^{-6}$ s^{-1}	4.3 %	0.010	1.2 %
180 °C	$8.3{\cdot}10^{-6}$ s^{-1}	9.7 %	0.008	1.0 %
190 °C	$1.6{\cdot}10^{-5}$ s^{-1}	5.2 %	0.002	0.2 %

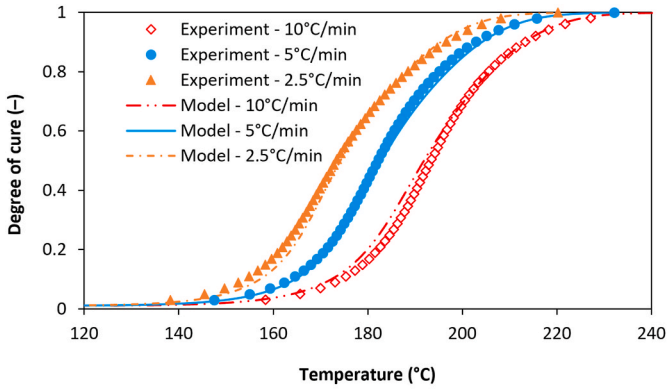


Fig. 6. Cure kinetics modelling of DHPDS-a: Comparison of model and experiment degree of cure evolution in dynamic (a) and isothermal (b) conditions.

basis of process development for the DHPDS-a system. It is specific to the dynamic bonds involved in this formulation and captures their overall effect on the kinetics.

Fig. 7 presents the rheological behaviour of DHPDS-a during the cure at 130°C and 150°C. In conventional thermosetting systems, the viscosity typically increases sharply once it reaches approximately 10 kPa·s, marking the onset of gelation. However, in DHPDS-a, the viscosity exhibits a distinct plateau beyond this threshold rather than a rapid increase. This behaviour indicates the occurrence of dynamic disulphide bond exchange, which enables continuous network rearrangement and stress relaxation even as the crosslink density increases. Since the advancing glass transition temperature remains below the measurement temperature within the time of the experiment, and the topology freezing temperature (≈78°C) is well below the curing temperatures studied, the system remains capable of bond exchange throughout the measurement. Consequently, the viscosity does not rise sharply after reaching the conventional gel point criterion but instead stabilises, reflecting the viscoelastic flow characteristics of vitrimers rather than irreversible gelation typical of thermosets.

As shown in Fig. 7(c), three regions can be distinguished from the graphs: a region of crosslinking dominance up to approximately 12 min in the 150°C experiment and approximately 45 min in the 130°C experiment, a region of bond exchange dominance (between 12 and 80 min in the 150°C measurement and 45–160 min in the 130°C measurement), and a region of vitrification dominance (after 80 min in the 150°C experiment and a time well after 160 min in the 130°C experiment). Under curing at 130–150°C ($\gg T_v$), the rapid disulphide exchange maintains viscoelastic flow and suppresses gelation; consequently, the rheological manifestation of gelation is obscured by dynamic exchange until vitrification dominates.

3.3. Glass transition temperature evolution

The experimental measurements of T_g for different states of cure of the DHPDS-a vitrimer are illustrated in Fig. 8 alongside the fitting of the DiBenedetto curve (Eq. (4)), with points corresponding to different isothermal and dynamic thermal histories for attaining the partial cure state. The values of T_g follow a single curve, reinforcing the conclusion that material state is defined by the degree of cure. The T_g varies over a wide temperature range from a monomer T_g of 22°C to an ultimate T_g of 155°C for the fully cured polymer. The high ultimate T_g of 155°C is characteristic of polybenzoxazines and renders the material applicable to high-temperature applications. Table 4 reports the values of the three model parameters obtained by fitting. The model reproduces experimental data closely with average error of 0.7 %, R^2 of 1.000, and a concave curve, due to a λ value of 1.84, which agrees with the λ value for a similar benzoxazine without a dynamic bond [25].

The value of λ for epoxy systems usually lies in the range $0< \lambda <1$ [36,37], corresponding theoretically to the ratio $\frac{\Delta C_{p\infty}}{\Delta C_{po}}$, where $\Delta C_{p\infty}$ and ΔC_{po} represent the step in specific heat capacity at glass transition for the fully cured polymer and the uncured prepolymer, respectively. A monomer has higher entropy than its polymer, due to the higher configurational degrees of freedom of the monomer relative to the polymer. Therefore, for epoxy systems, the enthalpy relaxation associated with glass transition is lower in the polymer than in the monomer, and $\Delta C_{p\infty} < \Delta C_{po}$, making their quotient lower than one. The values of λ reported in this work and those reported in Ref. [25] indicate that benzoxazines do not follow this behaviour. The value of λ greater than unity can be attributed to the complex nature of crosslinking of benzoxazines. Ishida [32] suggested that this could arise from intense intra and intermolecular hydrogen bonding by multifunctional hydroxyl groups from oligomeric benzoxazines during low conversion regime of polymerisation, faster development of molecular weight of intermolecularly hydrogen bonded molecules compared to weight development based only on covalent bonding, and strong stiffening effects of chelated intramolecular hydrogen bonding (O–H–N). These result in a faster

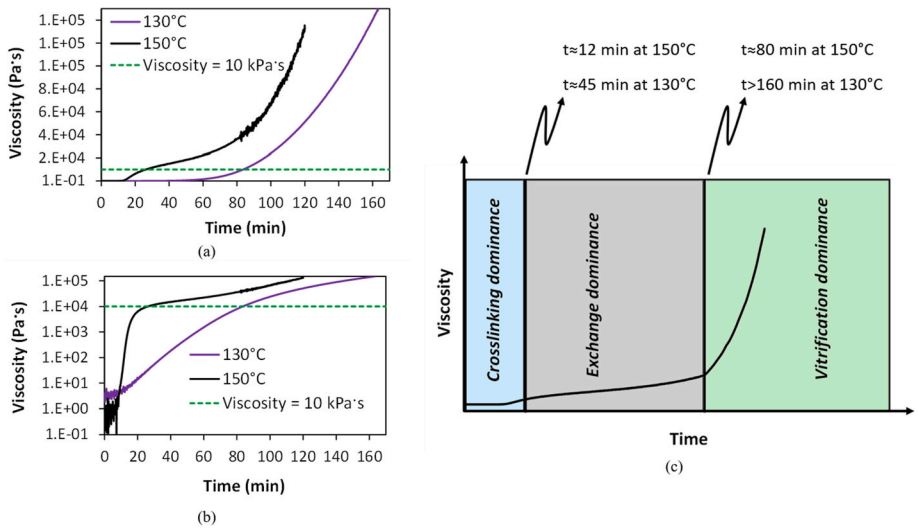


Fig. 7. Rheological behaviour of DHPDS-a during cure. (a) Viscosity versus time. (b) Viscosity in log scale versus time. (c) Regimes of dominance of crosslinking, bond exchange, and vitrification.

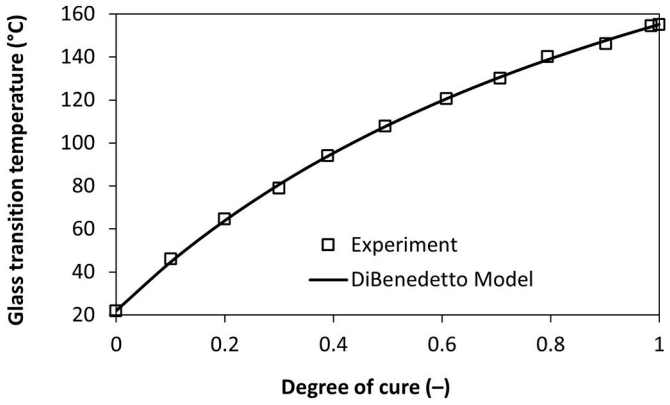


Fig. 8. Dependence of glass transition temperature of DHPDS-a vitrimer on degree of cure.

Table 4
DHPDS-a DiBenedetto T_g development model parameters and error.

$T_{g\infty}$ (°C)	T_{g0} (°C)	λ (–)	Average absolute error (°C)
155.16	22.00	1.84	0.77

development of glass transition temperature at low fractional conversion than at higher fractional conversion, a direct opposite of the case of epoxy resins, which typically produce one hydroxyl group per repeat unit of epoxide ring, in which glass transition temperature advancement is slowest at the beginning of cure and fastest post-vitrification [32,38]. These points suggest that the conventional interpretation of λ in terms of ΔC_p ratios may not be directly applicable to benzoxazines. The actual relationship between λ and specific heat capacity changes during glass transition of monomeric and polymeric benzoxazines need to be explored further. The most acceptable interpretation is that $\lambda > 1$ in benzoxazines is an empirical curvature parameter reflecting the nature of non-linear restriction of mobility arising from complex cure chemistry and network structure, which may not correspond to the conventional interpretation of λ.

A λ value above unity has important implications for the processing and application of the vitrimer. First, the steep rise in T_g with increasing degree of cure suggests that vitrification occurs abruptly upon network formation, imposing a narrower processing window and necessitating precise control of cure kinetics to prevent premature vitrification. This is evident in Fig. 6, where abrupt diffusion-controlled kinetics can be observed. Second, the rapid transition from a frozen to a flowable state above T_g—driven by fast disulphide metathesis—renders the cured network highly reprocessable at elevated temperatures. Notably, since the system fully relaxes stress within 5 s at 190°C [27], fibre-reinforced composites made from this vitrimer can be reprocessed at this temperature under practical composite consolidation pressures (≤10 bar) [1], due to the intrinsic malleability of the network, which has not been achieved with any high-T_g vitrimer. This enables thermoplastic-like operations such as remoulding, welding, reshaping, and 3D printing, creating new opportunities for reconfigurable or repairable polymer and composite systems. Finally, as the material remains chemically cross-linked but topologically dynamic above T_g, this duality must be incorporated into viscoelastic and stress evolution models, particularly for structural applications subject to thermal cycling or sustained mechanical loading.

Glass transition temperatures of the cure kinetics samples partially cured isothermally at 150 and 160°C were determined by running second DSC scans and found to be 145 and 148°C, respectively. The cure kinetics model developed in this study predicts degree of cure of 0.87 and 0.94, respectively for these samples, whilst 0.82 and 0.97 are the values determined from integrating DSC cure exotherm. Inputting these conversions into the DiBenedetto model gives glass transition temperatures of 145 and 151°C, thus confirming that cure kinetics model and DiBenedetto model are consistent.

The ultimate T_g of this vitrimer is 155°C. Isothermal curing at 150 and 160°C leads to incomplete conversions of 0.82 and 0.97, respectively. Lowering the curing temperature further would lead to earlier vitrification and even lower conversion. Curing at lower isothermal temperatures than 150°C would give the same kinetics, but the degree of cure is expected to be low, similar to BA-a, where conversion is approximately 0.5 for curing 17°C below the glass transition temperature [25]. Partial curing of samples for modelling the evolution of glass transition temperature was carried out using 1.25°C/min heating rate. Using degrees of cure predicted by cure kinetics model, the glass transition temperature evolution model yields values that match those measured by DSC, thereby reinforcing the validity of the overall modelling framework.

Fig. S4 and S5 in the supplement show the T_gs of mateiral cured isothermally at 150 and 160°C, respectively and part of residual heats. The degree of cure achieved after curing at 150°C is 0.82, accounting for

heat of reaction of 192.5 J/g, with about 41 J/g expected in the residual heat. The thermogram of Fig. S4 stopped around 198°C, recovering 8.2 J/g with the remaining 32 J/g lost to the unseen part of the thermogram, as the primary aim of the run wasto check $T_g - \alpha$ relation in the DiBenedetto equation. In Fig. S5, the residual energy is expected to be much lower, given the material has attained 0.97 degree of cure. Although only 2.8 J/g was recovered out of the balance of about 7 J/g (since the thermogram stopped at around 198°C), the remaining part of the thermogram accounts for about 4.2 J/g enthalpy.

3.4. Chemo-rheological modelling

The evolution of viscosity of DHPDS-a at typical isothermal infusion temperatures and the results of fitting the chemoviscosity data into Eqs. (5) and (6) is illustrated in Fig. 9 up to viscosities of 5 Pa·s. Due to increased molecular mobility with increasing temperature, the initial viscosity decreases with increasing temperature. The initial viscosity at 100°C is 1.12 Pa·s and reduces to 145 mPa·s at 130°C. The increase of viscosity with time is exponential, whilst the time spent at low viscosity is a decreasing function of temperature due to the acceleration of cross-linking with increasing temperature. At 100°C, 110°C and 120°C, the viscosity is greater than values typically required for liquid moulding (10–200 mPa·s). The material viscosity at 130°C is initially below 200 mPa·s but exceeds this limit within 2 min at this temperature.

Assuming a practical upper-limit viscosity of 2000 mPa·s at typical infusion temperatures (100–130°C)—above which fibre impregnation becomes difficult under normal consolidation pressures—the time required to reach this viscosity within the 100–130°C range was estimated to be 13–25 min. This relatively rapid viscosity build-up indicates that liquid composite moulding using in-plane infusion would be impracticable for this benzoxazine vitrimer, as the loss in flowability would lead to incomplete fibre wet-out.

In contrast, composites can be produced using resin film infusion or pre-impregnation with infusion/consolidation temperatures in the 100–120°C range. In Fig. 9, the data are equally spaced in terms of time and the error normalised with respect to the number of points in each experiment to ensure even coverage of all parts of the experimental envelope in the fitting.

The fitting shown in Fig. 9 follows closely the experimental data for all curves, with deviations observed only for the 110°C experiment, for which the model overestimates viscosity at the later stages of the process. The average absolute error is in the range of 14–84 mPa·s with an average of 34 mPa·s over all tests, representing relative error in the range of 3.3–21.3 %. This corresponds to an average relative error of 8.3 % and R^2 of 0.945, influenced by high error of 110°C experiment. This high error observed in 110°C experiment (21.3 %) does not invalidate the model, given the overall error of 8 %.

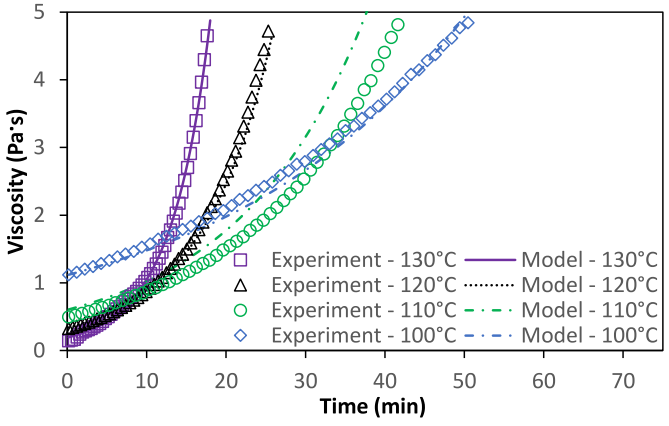


Fig. 9. Viscosity evolution of DHPDS-a over time at various isothermal temperatures and comparison of model to experiment.

At the end of the 100°C chemorheological experiment, the predicted extent of reaction is 0.01 corresponding to a viscosity of 6.5 Pa·s. The extents of reaction at the end of 110, 120, and 130°C chemorheological experiments are 0.02, 0.03, and 0.04, respectively, corresponding to viscosities of 9.89, 9.92, and 9.95 Pa·s, respectively. Although the extent of reaction is very low within the time window of each experiment, the rapid increase in viscosity observed in Fig. 9 implies a fast increase in polymerisation, which excludes the possibility of injection as also suggested by the $T_g - \alpha$ relation with λ greater than 1. The model parameters are summarised in Table 5 whilst the chemorheological model error and the degree of cure predicted by the cure kinetics model after each chemorheological experiment are presented in Table 6.

The chemorheological model reported in this study is suitable for the infusion and/or consolidation step of composites manufacturing during which matrix flow is critical. At this stage, models depending on cure conversion or instantaneous glass transition temperature, such as the Castro-Makosco equation [39], WLF equation, and its variants [40,41] do not accurately represent viscosity evolution because the rheological behaviour as represented by the model at low degrees of cure is dominated by evolution at greater degrees of cure and values of viscosity [42,43]. The use of viscosity at a reference temperature as the state variable governing the evolution of rheological behaviour overcomes this limitation [3,44].

Comparing the chemoviscosity of DHPDS-a vitrimer resin with commercial prepreg resins, it can be observed that DHPDS-a exhibits minimum viscosity of 100–300 mPa·s at 120–130°C, whereas for example Hexcel Composites EH25 epoxy prepreg resin features a minimum viscosity of 400–450 mPa·s in the same temperature range [45]. HexPly 8552— another aerospace epoxy prepreg resin—exhibits viscosity of 5500–8500 mPa·s at 120–130 °C [46]. These results show that DHPDS-a is significantly less viscous than established aerospace prepreg systems. Such low viscosity, whilst beneficial for fibre wetting, would increase the risk of uncontrolled resin flow and resin loss during curing if the neat resin were processed as produced. Accordingly, partial advancement to a B-stage would be required to achieve stable prepreg handling whilst preserving a suitable flow window during infusion.

Table 7 compares DHPDS-a with aerospace prepreg resins, high temperature conventional benzoxazine, aerospace-grade epoxy vitrimers, and disulphide-based benzoxazine vitrimer. DHPDS-a delivers a rare combination of high glass transition, low processing viscosity, and moderate cure temperature, closing much of the performance gap between benzoxazine vitrimers and aerospace epoxies whilst adding vitrimer functionalities such as reprocessability and repair.

4. Conclusions

The cure kinetics, glass transition temperature dependence on degree of cure and chemorheological modelling of an aerospace-grade benzoxazine vitrimer have been cestablished in this study. The models can be used to identify conditions for optimal manufacture of fibrous composites based on this benzoxazine vitrimer resin. The Karkanas equation, which is an autocatalytic model with two reaction rate constants and two nth reaction orders combined with a logistic function—accounting for diffusion regime of cure following resin vitrification—successfully simulates the matrix cure with an overall relative error in degree of cure prediction amounting to 4 %. Although the cure kinetics model developed in this study accurately simulates the cure behaviour of DHPDS-a, there is the need for more controlled synthesis of this benzoxazine vitrimer, carefully avoiding the observed oxazine ring preopening during

Table 5
DHPDS-a viscosity development parameters for Eqs. (5) and (6). Fitting performed for viscosity levels up to 5 Pa·s.

T_r (K)	η_r^0 (mPa·s)	A (s^{-1})	E (J mol^{-1})	l (–)	γ (mPa·s)	D (K^{-1})
373	1119	401,894	73,195	1.03	0.003	8760

Table 6
Degree of cure reached after each chemorheological experiment and average absolute and relative errors of the viscosity model of DHPDS-a.

Experiment	Degree of cure reached (−)	Absolute error (mPa·s)	Relative error
100 °C	0.011	17.1	3.8 %
110 °C	0.015	83.7	21.3 %
120 °C	0.021	14.5	3.3 %
130 °C	0.035	21.3	4.8 %

Table 7
Comparison of glass transition temperature, cure enthalpy, viscosity, and cure temperature of some high-temperature resin systems with those of DHPDS-a.

Resin system	$T_{g\infty}$ (°C)	ΔH_T (J/g)	η (mPa·s)	T_{cure} (°C)	Ref.
HexPly EH25 resin	180	–	400–450	180	[45]
HexPly 8552 resin	200	497–559	5500–8500	180	[46–48]
BA-a benzoxazine	177	309–328	≈10000	200	[20,25,33,49,50]
DGEBA/4-APDS	163	454.9	35	160	[3]
Aero-grade epoxy vitrimer	176	–	17–80	180	[51]
Cardanol–4-AFDS	40	–	200	195	[52]
DHPDS-a	155	236.2	100–300	170	This work

synthesis to quantify the suspected discrepancy in heat of reaction. Glass transition temperature depends on cure degree and varies from 22°C for the uncured resin to 155°C for the fully cured resin, in accordance with the DiBenedetto equation, featuring a concavity factor.

The chemoviscosity model accurately represents the evolution of rheological behaviour with an average error of 8.3 %. The range of viscosities and timings until viscosity reaches high levels show that the vitrimer is appropriate for film infusion/pre-impregnation processing. The models reported in this study will form the basis of process simulation and optimal manufacturing of thick fibrous aerospace composite laminates using DHPDS-a benzoxazine vitrimer matrix.

CRediT authorship contribution statement

Festus Ifeanyi Anagwu: Writing – review & editing, Writing – original draft, Visualization, Validation, Software, Resources, Project administration, Methodology, Investigation, Funding acquisition, Formal analysis, Data curation, Conceptualization. **Daniel Preston:** Validation, Formal analysis, Data curation. **Alex A. Skordos:** Writing – review & editing, Visualization, Validation, Supervision, Software, Resources, Project administration, Methodology, Funding acquisition, Formal analysis, Data curation, Conceptualization.

Declaration of competing interest

The authors declare that they have no known competing financial interests or personal relationships that could have appeared to influence the work reported in this paper.

Acknowledgements

This work received funding from the Tertiary Education Trust Fund [grant number TETF/ES/POLY/IMO STATE/TSAS/2019/VOL.I] and the European Union's Horizon Europe programme under grant agreement no. 101192721 (PLEIADES project).

Appendix A. Supplementary data

Supplementary data to this article can be found online at https://doi.org/10.1016/j.polymer.2025.129319.

Data availability

The dataset underlying this study is available through the Figshare research data repository at https://doi.org/10.6084/m9.figshare.28105523.

References

[1] F.I. Anagwu, Synthesis and Manufacturing of fibre-reinforced Vitrimeric Composites Based on Epoxy and Benzoxazine Matrices, Cranfield University, Thesis, 2024. https://dspace.lib.cranfield.ac.uk/handle/1826/24499. (Accessed 30 September 2025).
[2] B. Li, G. Zhu, Y. Hao, T. Ren, An investigation on the performance of epoxy vitrimers based on disulfide bond, J. Appl. Polym. Sci. 139 (2022) 51589, https://doi.org/10.1002/app.51589.
[3] F.I. Anagwu, A.A. Skordos, Cure kinetics, glass transition advancement and chemo-rheological modelling of an epoxy vitrimer based on disulphide metathesis, Polymer 288 (2023) 126427, https://doi.org/10.1016/j.polymer.2023.126427.
[4] V. Schenk, R. D'Elia, P. Olivier, K. Labastie, M. Destarac, M. Guerre, Exploring the limits of high-tg epoxy vitrimers produced through resin-transfer moulding, ACS Appl. Mater. Interfaces 15 (2023) 46357–46367, https://doi.org/10.1021/acsami.3c10007.
[5] T.A. Bogetti, J.W. Gillespie, Two-dimensional cure simulation of thick thermosetting composites, J. Compos. Mater. 25 (1991) 239–273, https://doi.org/10.1177/002199839102500302.
[6] S.R. White, Y.K. Kim, Staged curing of composite materials, Compos Part A Appl Sci Manuf 27 (1996) 219–227, https://doi.org/10.1016/1359-835X(95)00023-u.
[7] S.R. White, H.T. Hahn, Cure cycle optimization for the reduction of processing-induced residual stresses in composite materials, J. Compos. Mater. 27 (1993) 1352–1378, https://doi.org/10.1177/002199839302701402.
[8] X. Sun, L. Cook, J.P.-H. Belnoue, K.I. Tifkitsis, J. Kratz, A.A. Skordos, Manufacturing thick laminates using a layer by layer curing approach, Compos Part A Appl Sci Manuf 187 (2024) 108489, https://doi.org/10.1016/j.compositesa.2024.108489.
[9] L.G. Zhao, N.A. Warrior, A.C. Long, A micromechanical study of residual stress and its effect on transverse failure in polymer–matrix composites, Int. J. Solid Struct. 43 (2006) 5449–5467, https://doi.org/10.1016/j.ijsolstr.2005.08.012.
[10] M.M. Shokrieh, M. Safarabadi, Three-dimensional analysis of micro-residual stresses in fibrous composites based on the energy method: a study including interphase effects, J. Compos. Mater. 46 (2012) 727–735, https://doi.org/10.1177/0021998311410478.
[11] H.-L. Ma, K. Lau, D. Hui, S. Shi, C. Poon, Theoretical analysis on the pullout behaviour of carbon nanotube at cryogenic environment with the consideration of thermal residual stress, Compos. B Eng. 128 (2017) 67–75, https://doi.org/10.1016/j.compositesb.2017.07.009.
[12] J.M. Svanberg, J.A. Holmberg, An experimental investigation on mechanisms for manufacturing induced shape distortions in homogeneous and balanced laminates, Compos Part A Appl Sci Manuf 32 (2001) 827–838, https://doi.org/10.1016/S1359-835x(00)00173-1.
[13] H. Ghayoor, S.V. Hoa, C.C. Marsden, A micromechanical study of stress concentrations in composites, Compos. B Eng. 132 (2018) 115–124, https://doi.org/10.1016/j.compositesb.2017.09.009.
[14] J. Li, S.C. Joshi, Y.C. Lam, Curing optimization for pultruded composite sections, Compos. Sci. Technol. 62 (2002) 457–467, https://doi.org/10.1016/S0266-3538(02)00018-0.
[15] Z. Yuan, Y. Wang, G. Yang, A. Tang, Z. Yang, S. Li, Y. Li, D. Song, Evolution of curing residual stresses in composite using multi-scale method, Compos. B Eng. 155 (2018) 49–61, https://doi.org/10.1016/j.compositesb.2018.08.012.
[16] T. Rev, M.R. Wisnom, X. Xu, G. Czél, The effect of transverse compressive stresses on tensile failure of carbon fibre/epoxy composites, Compos Part A Appl Sci Manuf 156 (2022) 106894, https://doi.org/10.1016/j.compositesa.2022.106894.
[17] F. Zhang, Y. Ye, M. Li, H. Wang, L. Cheng, Q. Wang, Y. Ke, Computational modelling of micro curing residual stress evolution and out-of-plane tensile damage behaviour in fibre-reinforced composites, Compos. Struct. 322 (2023) 117370, https://doi.org/10.1016/j.compstruct.2023.117370.
[18] S. Zhao, L. Pei, H. Li, Y. Ma, Q. Lian, S. Zhou, G. Zhao, Z. Wang, Research progress in toughening modification of polybenzoxazine, Engineered Sci. (2020), https://doi.org/10.30919/es8d1150.
[19] H. Liang, H. Liu, Y. Chen, Y. Cui, T. Bu, Z. Wang, Enhancing the toughness of polybenzoxazines through multiple sacrificial bonds for improved overall performance, J. Mater. Res. Technol. 31 (2024) 659–667, https://doi.org/10.1016/j.jmrt.2024.06.085.
[20] H. Ishida, Y. Rodriguez, Curing kinetics of a new benzoxazine-based phenolic resin by differential scanning calorimetry, Polymer 36 (1995) 3151–3158, https://doi.org/10.1016/0032-3861(95)97878-j.
[21] C. Jubsilp, S. Damrongsakkul, T. Takeichi, S. Rimdusit, Curing kinetics of arylamine-based polyfunctional benzoxazine resins by dynamic differential scanning calorimetry, Thermochim. Acta 447 (2006), https://doi.org/10.1016/j.tca.2006.05.008.
[22] C.F. Bandeira, A.C. Pereira, E.C. Botelho, M.L. Costa, Benzoxazine resin and their nanostructured composites cure kinetic by DSC, J. Mater. Res. 28 (2013) 3094–3099, https://doi.org/10.1557/jmr.2013.327.

[23] A. Ručigaj, Š. Gradišar, M. Krajnc, Kinetic investigation of a complex curing of the guaiacol bio-based benzoxazine system, E-Polymers 16 (2016) 199–206, https://doi.org/10.1515/epoly-2015-0250.
[24] W. Bessa, D. Trache, C. Ghalmi, S. Aidi, A.F. Tarchoun, F. Gahfif, A. Abdelaziz, S. Thakur, M.H. Hussin, Curing kinetics of composites based on benzoxazine resin and microcrystalline cellulose modified by phosphorus salt, Thermochim. Acta 735 (2024) 179718, https://doi.org/10.1016/j.tca.2024.179718.
[25] V.V. Shutov, E.A. Gorbunova, I.Yu Gorbunova, I.S. Sirotin, Isoconversional kinetic analysis of bisphenol A benzoxazine cure, Thermochim. Acta 748 (2025) 179984, https://doi.org/10.1016/j.tca.2025.179984.
[26] L. Wang, Z. Lin, W. Xie, W. Shang, F. Bu, Y. Xu, S. Meng, Curing kinetic models of benzoxazine-modified phenolic triazine resin for the dynamic curing process, J. Appl. Polym. Sci. 142 (2025), https://doi.org/10.1002/app.57145.
[27] F.I. Anagwu, E. Dossi, A.A. Skordos, High glass transition catalyst-free polybenzoxazine vitrimer through one-pot solventless method, React. Funct. Polym. (2025) 106186, https://doi.org/10.1016/j.reactfunctpolym.2025.106186.
[28] P.I. Karkanas, K. Partridge, D. Attwood, Modelling the cure of a commercial epoxy resin for applications in resin transfer moulding, Polym. Int. 41 (1996) 183–191, https://doi.org/10.1002/(sici)1097-0126(199610)41:2<183::aid-pi621>3.0.co;2-f.
[29] K.C. Cole, J.J. Hechler, D. Noël, A new approach to modeling the cure kinetics of epoxy amine thermosetting resins. 2. application to a typical system based on bis [4-(diglycidylamino)phenyl]methane and bis(4-aminophenyl) sulfone, Macromolecules 24 (1991) 3098–3110, https://doi.org/10.1021/ma00011a012.
[30] D. Fylstra, L. Lasdon, J. Watson, A. Waren, Design and use of the microsoft excel solver, Interfaces 28 (1998) 29–55, https://doi.org/10.1287/inte.28.5.29.
[31] F.I. Anagwu, D. Preston, A.A. Skordos, Dataset for Cure kinetics, glass transition and chemoviscosity models for an aerospace-grade disulphide-based benzoxazine vitrimer, Figshare Res. Data Repos. (2025), https://doi.org/10.6084/m9.figshare.28105523.
[32] M. Kanchanasopa, N. Yanumet, K. Hemvichian, H. Ishida, The effect of polymerization conditions on the density and tg of bisphenol-a and hexafluoroisopropylidene-containing polybenzoxazines, Polym. Polym. Compos. 9 (2001) 367–376, https://doi.org/10.1177/096739110100900601.
[33] W.A. Wan Hassan, J. Liu, B.J. Howlin, H. Ishida, I. Hamerton, Examining the influence of bisphenol A on the polymerisation and network properties of an aromatic benzoxazine, Polymer 88 (2016) 52–62, https://doi.org/10.1016/j.polymer.2016.01.041.
[34] L. Dumas, L. Bonnaud, M. Olivier, M. Poorteman, P. Dubois, Chavicol benzoxazine: Ultrahigh Tg biobased thermoset with tunable extended network, Eur. Polym. J. 81 (2016) 337–346, https://doi.org/10.1016/j.eurpolymj.2016.06.018.
[35] F.I. Anagwu, V.K. Thakur, A.A. Skordos, High-performance vitrimeric benzoxazines for sustainable advanced materials: design, synthesis, and applications, Macromol. Mater. Eng. 308 (2023) 2200534, https://doi.org/10.1002/mame.202200534.
[36] J.P. Pascault, R.J.J. Williams, Glass transition temperature versus conversion relationships for thermosetting polymers, J. Polym. Sci. B Polym. Phys. 28 (1990) 85–95, https://doi.org/10.1002/polb.1990.090280107.
[37] R.A. Venditti, J.K. Gillham, A relationship between the glass transition temperature (Tg) and fractional conversion for thermosetting systems, J. Appl. Polym. Sci. 64 (1997) 3–14, https://doi.org/10.1002/(sici)1097-4628(19970404)64:1<3::aid-app1>3.0.co;2-s.
[38] R.A. Venditti, J.K. Gillham, E. Chin, F.M. Houlihan, Glass transition temperature (Tg) versus fractional conversion for a linear thermosetting polyamic acid ester–polyimide system, J. Appl. Polym. Sci. 53 (1994) 455–461, https://doi.org/10.1002/app.1994.070530408.
[39] C.W. Makosco, RIM, Fundamentals of Reaction Injection, Hanser Publishers, 1989.
[40] M.L. Williams, R.F. Landel, J.D. Ferry, The temperature dependence of relaxation mechanisms in amorphous polymers and other glass-forming liquids, J. Am. Chem. Soc. 77 (1955) 3701–3707, https://doi.org/10.1021/ja01619a008.
[41] P.I. Karkanas, I.K. Partridge, Cure modelling and monitoring of epoxy/amine resin systems. ii. network formation and chemoviscosity modelling, J. Appl. Polym. Sci. 77 (2000) 2178–2188, https://doi.org/10.1002/1097-4628.
[42] Q.P.V. Fontana, Viscosity: thermal history treatment in resin transfer moulding process modelling, Compos Part A Appl Sci Manuf 29 (1998) 153–158, https://doi.org/10.1016/s1359-835x(97)00048-1.
[43] N. Kiuna, C.J. Lawrence, Q.P.V. Fontana, P.D. Lee, T. Selerland, P.D.M. Spelt, A model for resin viscosity during cure in the resin transfer moulding process, Compos Part A Appl Sci Manuf 33 (2002), https://doi.org/10.1016/s1359-835x(02)00177-x.
[44] A.A. Skordos, Y.D. Kergomard, P. Marquette, P. De Luca, Methodology applied to integrate a viscosity model for liquid composites moulding simulation in PAM-RTM, in: ASME 2012 11th Biennial Conference on Engineering Systems Design and Analysis, American Society of Mechanical Engineers Digital Collection, Nantes, France, 2012, pp. 11–19, https://doi.org/10.1115/esda2012-82096.
[45] Hexcel, HexPly EH25 epoxy matrix product data sheet, hexcel. https://www.hexcel.com/user_area/content_media/raw/hexply_eh25_eu_datasheet.pdf, 2020. (Accessed 30 September 2025).
[46] Hexcel, HexPly 8552 epoxy matrix product data sheet, Hexcel. https://www.hexcel.com/user_area/content_media/raw/hexply_8552_eu_datasheet(1).pdf, 2023. (Accessed 29 September 2025).
[47] S.J. Ng, R. Boswell, S.J. Claus, F. Arnold, A. Vizzini, Degree of cure, heat of reaction, and viscosity of 8552 and 977-3 HM epoxy resin. https://doi.org/10.21236/ada377439, 2000.
[48] P. Hubert, A. Johnston, A. Poursartip, K. Nelson, Cure kinetics and viscosity models for Hexcel 8552 epoxy resin, in: 46th International SAMPE Symposium and Exhibition, SAMPE North America, California, 2001. https://www.nasampe.org/store/viewproduct.aspx?id=4318113. (Accessed 4 October 2025).
[49] J. Sun, W. Wei, Y. Xu, J. Qu, X. Liu, T. Endo, A curing system of benzoxazine with amine: reactivity, reaction mechanism and material properties, RSC Adv. 5 (2015) 19048–19057, https://doi.org/10.1039/c4ra16582a.
[50] L.M. Amirova, O.L. Khamidullin, G.M. Madiyarova, D.A. Balkaev, I.S. Antipin, R. R. Amirov, Novel carbon-fiber powder benzoxazine-epoxy composites, J. Polym. Res. 32 (2025) 135, https://doi.org/10.1007/s10965-025-04370-8.
[51] A. Ruiz de Luzuriaga, N. Markaide, A.M. Salaberria, I. Azcune, A. Rekondo, H. J. Grande, Aero grade epoxy vitrimer towards commercialization, Polymers 14 (2022) 3180, https://doi.org/10.3390/polym14153180.
[52] A. Trejo-Machin, L. Puchot, P. Verge, A cardanol-based polybenzoxazine vitrimer: recycling, reshaping and reversible adhesion, Polym. Chem. 11 (2020) 7026–7034, https://doi.org/10.1039/d0py01239d.